View metadata, citation and similar papers at core.ac.uk

brought to you by CORE

provided by Calhoun, Institutional Archive of the Naval Postgraduate School

Calhoun

Institutional Archive of the Naval Postgraduate School

Calhoun: The NPS Institutional Archive

Faculty and Researcher Publications

Faculty and Researcher Publications

1999

An Experimental and Numerical Investigation of Flapping-Wing Propulsion

Jones, K.D.

Jones, K.D. and Platzer, M.F., "An Experimental and Numerical Investigation of Flapping-Wing Propulsion," AIAA Paper No. 99-0995, 37th AIAA Aerospace Sciences Meeting, Reno, Nevada,

DUDLEY KNOX LIBRARY

http://www.nps.edu/library

Calhoun is a project of the Dudley Knox Library at NPS, furthering the precepts and goals of open government and government transparency. All information contained herein has been approved for release by the NPS Public Affairs Officer.

Dudley Knox Library / Naval Postgraduate School
411 Dyer Road / 1 University Circle
Monterey, California USA 93943

AIAA−99−0995
AN EXPERIMENTAL AND NUMERICAL INVESTIGATION OF FLAPPING−WING PROPUSLSION

K.D.Jones and M.F.Platzer
Naval Postgraduate School
Monterey, CA

37th Aerospace Sciences Meeting & Exhibit
January 11−14,1999 / Reno, NV

For permission to copy or republish, contact the American Institute of Aeronautics and Astronautics 1801 Alexander Bell Drive, Suite 500, Reston, VA 20191

AN EXPERIMENTAL AND NUMERICAL INVESTIGATION OF FLAPPING-WING PROPULSION

K. D. Jones[†] and M. F. Platzer[‡]

Naval Postgraduate School
Monterey, California

Abstract

Flapping-wing propulsion is investigated experimentally and numerically with direct comparisons between experimental and numerical thrust measurements for several geometrically simple configurations. Numerical simulations are performed using linear theory, and a previously developed, unsteady panel method that models one or two independently moving airfoils with three-degrees of freedom and non-linear deforming wakes. Experiments are carried out in the Naval Postgraduate School $5' \times 5'$ low-speed tunnel. A flapping mechanism that approximates the two-dimensional motions modeled by the panel code is suspended with cables in the wind tunnel, and thrust measurements are made by measuring the streamwise displacement of the model using a laser range-finder. The experimental flapping mechanism utilizes variable aspect-ratio wings and optional tip plates to investigate the effect of three-dimensionality. The device flaps two airfoils, each with two degrees of freedom and adjustable pitch and plunge amplitudes, and additional stationary wings may be attached up and/or downstream of the flapping wings to investigate interference effects.

Nomenclature

b = wing span
c = chord length
C_d = drag coefficient per unit span, $D/(q_\infty c)$
C_l = lift coefficient per unit span, $L/(q_\infty c)$
C_m = moment coefficient per unit span, $M/(q_\infty c^2)$
C_p = power coefficient per unit span, $-C_l\dot{y} - C_m\dot{\alpha}$
C_t = thrust coefficient per unit span, $T/(q_\infty c)$
D = drag per unit span
f = frequency in Hertz
h_x = horizontal plunge amplitude in terms of c
h_y = vertical plunge amplitude in terms of c
k = reduced frequency, $\omega c/U_\infty$
L = lift per unit span
M = moment per unit span
q_∞ = freestream dynamic pressure, $1/2\rho_\infty U_\infty^2$
R_L = chord Reynolds number, $U_\infty c/\nu_\infty$
Sr = Strouhal number, $\omega h_y c/U_\infty$
t = time
T = thrust per unit span $(-D)$
U_∞ = freestream velocity
x_p = pivot location from LE in terms of c
$x(\tau)$ = horizontal displacement in terms of c
$y(\tau)$ = vertical displacement in terms of c
α = angle of attack
$\Delta\alpha$ = pitch amplitude in degrees
ϕ_x = phase between pitch and horizontal plunge
ϕ_y = phase between pitch and vertical plunge
η = propulsive efficiency, C_t/C_p
λ = wake wavelength in terms of c
ν_∞ = freestream kinematic viscosity
ω = circular frequency, $2\pi f$
ρ_∞ = freestream density
τ = nondimensional time, tU_∞/c
$(\dot{\cdot})$ = rate of change w.r.t. τ

Introduction

Knoller[1] and Betz,[2] in independent studies in 1909 and 1912, respectively, were the first ones to observe that a flapping wing creates an effective angle of attack, resulting in a normal-force vector with both lift and thrust components. Katzmayr[3] provided the first experimental verification of the Knoller-Betz effect in 1922 when he placed a stationary airfoil into a sinusoidally oscillating wind stream and measured an average thrust. In 1924, Birnbaum[4,5] identified the conditions which lead to flutter or to thrust generation. He also suggested the use of a sinusoidally flapping (plunging) wing as an alternative to the conventional propeller.

In the following decade the aerodynamics of plunging and pitching airfoils received much attention because of its importance for reliable flutter and gust-response analyses. However, such analyses only required the determination of the lifting forces generated by plunging or pitching airfoils and, consequently, little effort was devoted over the years to the determination of the thrust forces. Nevertheless, in 1935 von

---

[†] Assistant Research Professor, Senior Member, AIAA
[‡] Professor, Associate Fellow, AIAA

This paper is declared a work of the U.S. Government and is not subject to copyright protection in the United States.

Kármán and Burgers[6] offered the first theoretical explanation of drag or thrust production based on the observed location and orientation of the wake vortices, as illustrated in Figs. 1 and 2 for drag-indicative and thrust-indicative wakes, respectively.

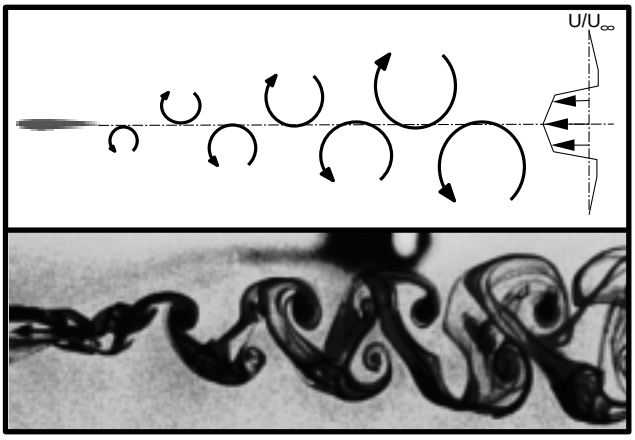

Fig. 1: Drag producing vortex street.[7]

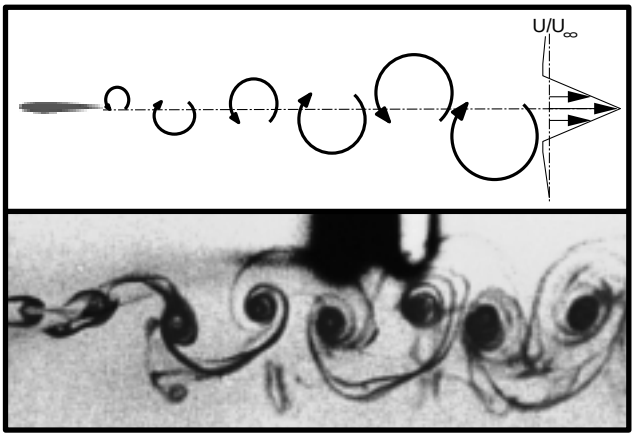

Fig. 2: Thrust producing vortex street.[7]

At about the same time, Garrick[8] applied Theodorsen's inviscid, incompressible, oscillatory, flat-plate theory[9] to the determination of the thrust force and showed that plunging airfoils generate thrust over the whole frequency range, whereas pitching airfoils do so only with frequencies above a certain critical value and as a function of the pivot location. To some this may have seemed obvious, since a fluttering airfoil extracts energy from the flow and, therefore, must create drag not thrust (according to linear theory, an oscillating airfoil either flutters or produces thrust). Theodorsen showed that pitching airfoils could flutter only at low frequencies and plunging airfoils would never flutter.

In 1939, Silverstein and Joyner[10] provided the first experimental verification of Garrick's prediction, and in 1950 Bratt[11] performed flow visualization experiments which corroborated von Kármán and Burgers' observations. Of particular interest, Bratt's experimental data included several cases where a non-symmetrical, deflected wake pattern was recorded, but no comment was made on these deflected wakes, and, in fact, they were never again reported until Jones et al.[7] where they were shown to be reproducible both numerically and experimentally.

Birnbaum's suggestion to regard a flapping foil as an alternative (two-dimensional) propeller generated some interest over the years. Most noteworthy is Kuchemann and Weber's book[12] in which they comment on aerodynamic propulsion in nature and observe that the propulsive efficiency of an idealized flapping wing is greater than that of a simplified propeller model because of the disadvantageous trailing vortex system generated by the propeller.

It was recognized that at reasonable frequencies a large portion of the energy used to flap the airfoil was lost in the form of vorticity shed in the wake, and in 1942 Schmidt[13] discovered a method for recovering some of the vortical energy released from a flapping airfoil. He demonstrated that improved propulsive efficiencies could be achieved by placing a stationary airfoil in the oscillatory wake of a flapping airfoil. Obvious mechanical difficulties arise from pure plunging motions, and Schmidt addressed this difficulty by developing his *wave propeller*, shown in Fig. 3, where the lead airfoil is moved in a circular path with a fixed angle of attack creating an oscillating flowfield for the second airfoil.

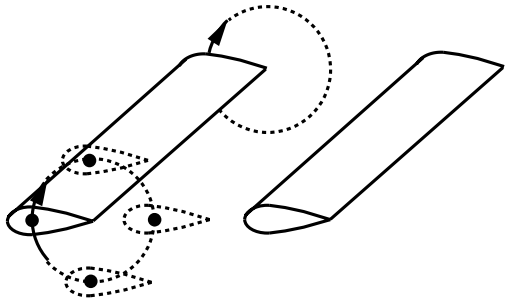

Fig. 3: The Schmidt *wave propeller*.

Schmidt demonstrated his wave propeller on a catamaran boat and claimed propulsive efficiencies comparable to those obtained with conventional propellers.

In 1977, Bosch[14] developed a linear theory for predicting propulsion from flapping airfoils and airfoil combinations, for the first time including wake interference effects in propulsive efficiency computations, and in 1982 DeLaurier and Harris[15] obtained experimental measurements of flapping-wing propulsion.

Thrust production due to pitching motions was experimentally demonstrated by Koochesfahani[16] in 1989. Unlike plunging foils, which produce thrust for

all frequencies, pitching foils produce drag for very low frequencies, a feature that leads to pitch-instability or flutter. In the case of flutter, energy is extracted from the flow, creating a drag profile in the wake of the foil and amplifying the motion of the foil.

More recently, the problem of flapping foil propulsion has been considered by Liu[17,18] using vortex lattice and panel methods, by Send[19,20] using linearized theory and by Hall and Hall[21] and Hall et al.[22] using vortex lattice methods. Jones et al.[7] compared wake structures behind flapping wings experimentally photographed and numerically predicted, and demonstrated that the formation and evolution of these unsteady wakes is essentially an inviscid phenomenon over a broad range of Strouhal numbers. Jones and Platzer[23] performed extensive numerical flapping-wing propulsion calculations using panel methods, and found a large performance enhancement for an airfoil flapping in ground effect, an effect often utilized by birds.

Virtually all past numerical studies in flapping-wing propulsion considered inviscid flows, or ignored skin-friction drag in the performance estimates. Likewise, very few experimental studies provided quantitative thrust measurements with which direct comparisons to numerical methods could be made.

It is the purpose of this investigation to directly compare experimental and numerical thrust measurements for several geometrically simple configurations, and to experimentally investigate more complex, multi-element configurations, as well as the effects of three-dimensionality and flow-separation.

Numerical simulations are performed using linear theory, and a previously developed, unsteady panel method that can model one or two independently moving airfoils with three-degrees of freedom and non-linear deforming wakes. The numerical methods are two-dimensional, incompressible and inviscid. As will be shown, flapping-wing propulsion is only useful at low speeds, so the use of incompressible theory is adequate. The effect of flow viscosity is addressed on one hand by adding a profile drag coefficient to the numerical thrust calculations, and on the other hand by subtracting the steady profile drag from the experimentally measured thrust.

Experiments are carried out in the Naval Postgraduate School $5' \times 5'$ low-speed tunnel. A flapping mechanism that approximates the two-dimensional motions modeled by the panel code is suspended with cables in the wind tunnel and thrust measurements are made by measuring the streamwise displacement of the model using a laser range-finder. The experimental flapping mechanism is designed so that variable aspect-ratio wings may be used to investigate the effect of three-dimensionality. The device flaps two airfoils, each with two degrees of freedom and adjustable pitch and plunge amplitudes, and additional stationary wings may be attached up and/or downstream of the flapping wings to investigate interference effects similar to Schmidt's *wave-propeller*.

In the following sections, the experimental and numerical methods are described in detail, and numerical and experimental data are evaluated and compared over a limited range of the immense parameter space.

Methods

The experimental and numerical methods utilized in this study are briefly described in the sections below. Additionally, the numerical and experimental configurations and the unsteady motions are described.

Experimental Methods

Isometric, side and top views of the experimental flapping-wing mechanism are shown in Figs. 4-6, respectively. The device is constructed primarily from aluminum, with balsa-wood nacelles at the front and rear. The mechanism allows for two moving airfoils, each with two degrees of freedom and adjustable pitch and plunge amplitudes. Additionally, fixed airfoils may be attached to the mechanism both ahead of and behind the flapping wings with adjustable location, as illustrated in the top view (Fig. 6).

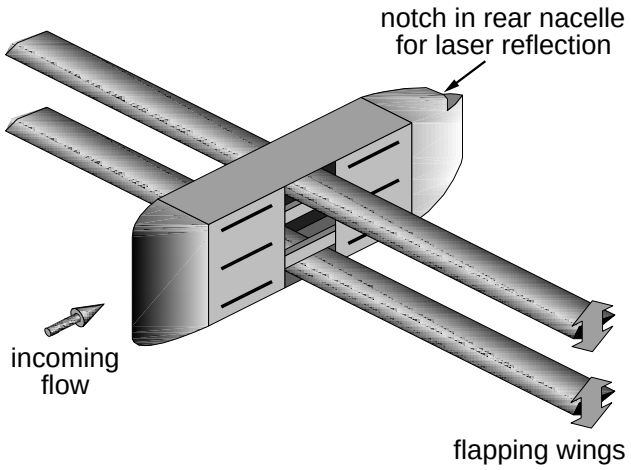

Fig. 4: Isometric view of the flapping mechanism.

The flapping wings are attached to moving beams that are actuated by the large wheels, shown in Fig. 5, by means of bearinged pins that are bolted through the slots in the beams, into the rotating wheels. As the wheels rotate the beams are forced up and down. The amplitude of the motion is determined by the radius of the hole the pins are screwed into, and the mode of the motion (pitch/plunge) is determined by

the phasing between the fore and aft actuation wheels.

The actuation wheels are driven using worm gears, and the unit is coupled to an Astro-Flight Cobalt 40 motor. A variable current/voltage power supply is used, with a voltage range of 0-30 volts, and a current range of 0-25 amps. The motor is limited to 25 volts, and it typically draws about 5 amps during operation. The maximum flapping frequency is approximately 8 Hz, which, through the 50-to-1 gear ratio, corresponds to a motor speed of 24,000 RPM.

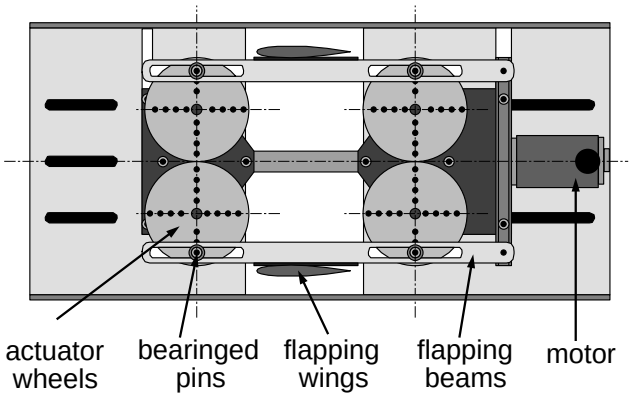

Fig. 5: Side view w/o left side plates and nacelles.

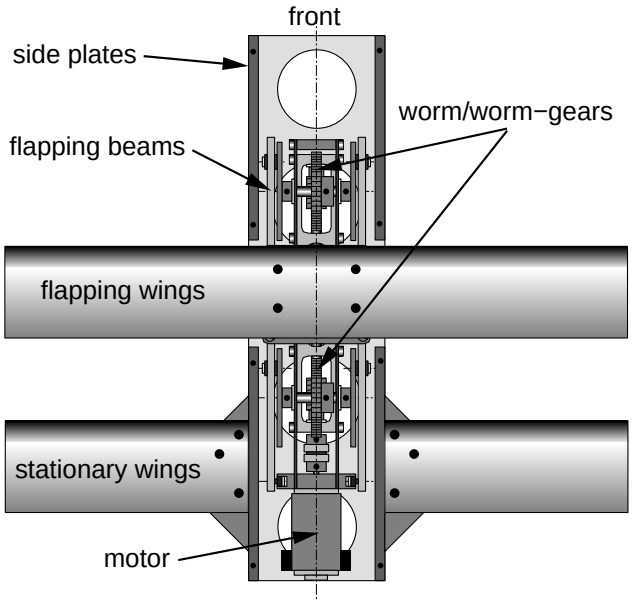

Fig. 6: Top view w/o top plate and nacelles.

The flapping frequency is measured using a strobe light. Typically the strobe light is set to the desired frequency, and the motor voltage is adjusted such that the flapping-wings appear to be stationary. The strobe-rate is set by a large dial, with 1/60 Hz gradient marks in the 0-6 Hz range, and 1/12 Hz marks in the 6-8 Hz range. Using the strobe's cross-hair, it is estimated that that the strobe rate can be set to within 1/120 Hz in the slow range, and within 1/48 Hz in the high range. While adjusting the speed of the motor, typically the position of the actuation wheels is observed for 4 or 5 seconds, with an estimated motion of less than 10 degrees. This corresponds to a worst case frequency error of about 1% in the low range and about 3% in the high range.

A variety of wings can be bolted to the flapping mechanism. Wings with both symmetric (resembling a NACA 0014 section) and asymmetric (resembling a NACA 23012) section, with aspect ratios between 10 and 20 have been obtained. The wings are manufactured by the Miniature Aircraft Supply model helicopter company, and are constructed of laminated hardwoods and balsa wood, covered with a thin plastic film. All of the experimental results presented here are for the symmetric airfoil with an aspect ratio of 20. The wings have a chord length of approximately $64mm$ and a span of $1270mm$. The fuselage has a width of about $70mm$, providing a useful lifting-span of $1200mm$ (used as the span in the numerical model when computing thrust values).

Experiments are performed in the Naval Postgraduate School $5' \times 5'$ low-speed wind-tunnel, shown in Fig. 7. The tunnel, modeled after the one described in Ref. 24, is a continuous, flow-through facility with an approximate flow speed range between $3m/s$ and $14m/s$. The speed is set by varying the pitch of a fan which is driven by a constant speed motor. The tunnel has a square, $15' \times 15'$, bell-shaped inlet with a 9-to-1 contraction ratio to the $5' \times 5'$ test section. The turbulence level has been determined by Costello[25] using a hot-wire anemometer. In the speed range from 6 fps to 32 fps the highest level was 0.97% and the lowest level was 0.47%.

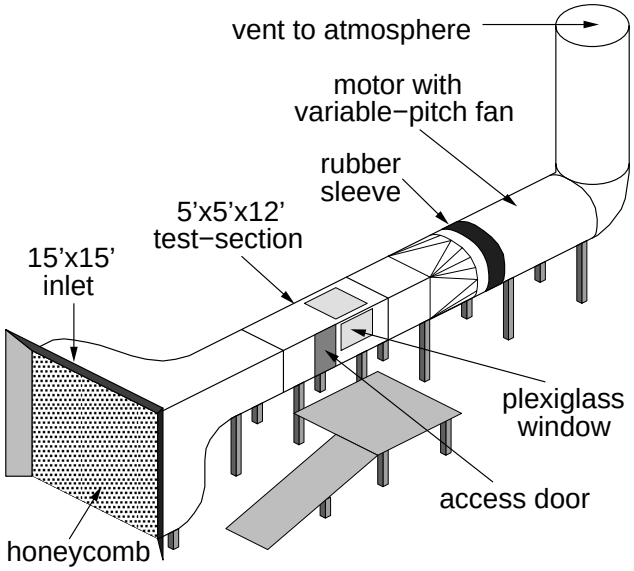

Fig. 7: The NPS low-speed wind tunnel.

The model is suspended from the ceiling with 4 thin cables that are attached to rails bolted into the ceiling, as shown in Fig. 8. The cables allow the model to swing in the streamwise direction, but keep it very stable in all other directions. When drag or thrust is present, the model is displaced, and the displacement is measured using a laser range-finder with the laser reflected off of a flat surface in a notch that is cut into the rear nacelle, as shown in Figs. 4 and 8. The laser is mounted to a 2-axis translation table positioned downstream of the model, as shown in Fig. 8.

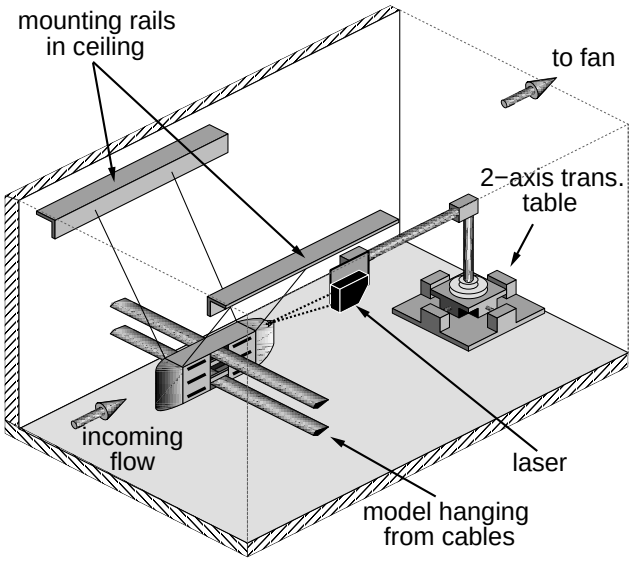

Fig. 8: The flapper mounted in the test section.

The flapping mechanism was designed to be robust and reliable, and was not meant to be a flying vehicle. Consequently, weight was not an important factor in its design. The full mechanism weighs about 4 kg, and therefore, the displacements are relatively small, on the order of a few centimeters. The laser analog sensor (NAIS, model ANL1651), reflects a laser off of a surface between 80 and $180mm$ from the sensor, and produces an analog voltage of $1V/cm$. The voltage is measured with a Hewlett Packard 100MHz oscilloscope (model 54600B). The laser has a resolution (2σ) of $40\mu m$, which corresponds to roughly ± 0.0016 Newtons.

The displacement was computed using the average measured voltage over a 10 second period, which covered between 20 and 80 flapping oscillations for the experiments. During a series of measurements, the neutral (non-flapping) location was measured 4 times, and the standard deviation of these measurements was on the order of 0.010 volts. Assuming a 2σ error band, this corresponds to roughly ± 0.0005 Newtons. The total estimated error in the thrust measurements is roughly ± 0.0021 Newtons.

Calibration of the setup is performed by hanging known weights on a thread that goes over a pulley and attaches to the model, and measuring the displacement of the model. Calibration measurements demonstrate a very nearly linear displacement/force response. Calibration curves must be made for each configuration tested, since the mass of the model changes.

The mechanical pitch and plunge amplitudes can be measured precisely by measuring the radius of the pins and the phasing of the wheels, however, especially at higher frequencies, the long slender wings tend to flex, significantly increasing the plunge amplitude at the tip. This increase in plunge amplitude can be estimated with reasonable accuracy, using the strobe light to view the wing positions anywhere in the cycle. As will be seen from the results, some torsional flexing is suspected but is, as yet, unmeasurable.

Flow speed in the tunnel is presently measured using a pitot-static tube at the upstream end of the test-section, attached to a micro-manometer. A Dantec LDV system is being installed, and this will provide a second, more accurate means for velocity measurements. Unfortunately, the LDV equipment could not be installed in time to be of use in this investigation.

The micro-manometer (Flow Corporation, Model MM-2) is basically an elegant version of the classic, U-shaped glass tube manometer where the static and total pressure are attached to opposite sides of the tube, and the velocity is determined by the displacement of fluid in the tube. The velocity is given by

$$U_\infty = \sqrt{4\rho_l g \Delta h / \rho_\infty} \qquad (1)$$

where ρ_l is the fluid density, and Δh is the change in fluid height on one side of the tube.

Several factors contribute to the error associated with velocity measurements; the accuracy of the pitot-static tube, the accuracy of the micro-manometer and the accuracy of the air and fluid densities.

The pitot-static tube has errors associated with the measurement of both the static and total pressure. The pitot tube used here has an outer diameter of 0.25 inches, 8 static ports aligned symmetrically, 2 inches (8 diameters) downstream of the tip, and a stem approximately 4.5 inches (18 diameters) downstream of the static ports. According to Pope,[26] the geometry of the probe should yield about an 0.5% over-prediction of the static pressure. Additional errors may occur from misalignment of the probe, but with a 6 degree misalignment the error is estimated to be about 0.5%. A one percent error in the prediction of the dynamic pressure, used in Eq. (1), yields roughly a 0.5% error in the velocity prediction.

The micro-manometer is quite accurate. The fluid level is measured using a micrometer with 0.0001

inch increments. It was found that the fluid level could be measured repeatedly to within about ± 0.0002 inches which, due to the square-root relationship of Δh in Eq. (1), corresponds to about $\pm 0.020 m/s$ at $3.2 m/s$, the lowest speed obtained, and $\pm 0.005 m/s$ at $7.5 m/s$, the highest speed obtained. This is a 0.6% error at the low-speed limit, and a 0.1% error at the high-speeds limit.

The air density was determined from the static temperature and pressure, and the fluid (low vapor-pressure, isopropyl alcohol) density was obtained from Pope.[26] The wind-tunnel is a flow-through design which draws air from the rest of the building. After the tunnel is run for some time, the air in the building is replaced by air drawn from outside the building, and the temperature and pressure change slightly. The largest density variation recorded corresponded to a velocity error of about 0.8%. The fluid used is isopropyl alcohol with greater than 99% purity. The sensitivity to temperature, according to Pope, is rather severe, but the fluid temperature never changed more than a degree or two during a series of measurements. The velocity error associated with this is estimated to be about 0.3%.

An additional error contribution was derived from the drawing of air from the building. As doors and windows were opened and closed in other parts of the building, the velocity had a tendency to drift slightly during a series of measurements. Systematic measurements of the pressure provided a means of estimating the velocity error incurred from this. The standard deviation, σ, of a typical series of measurements of Δh is on the order of 0.0004 inches at the low-speed end, and 0.0013 inches at the high-speed end. Thus, a 2σ error corresponds to roughly a 2.2% error at low speeds, and a 0.4% error at high speeds.

The total velocity error-bound, including all the above mentioned factors, is estimated at about $\pm 4.4\%$ at low speeds, down to about $\pm 2.1\%$ at high speeds. This assumes that all the errors act in the same direction, whereas, in reality some of them may cancel each other out.

For oscillatory motions the reduced frequency and/or Strouhal number are generally the significant non-dimensional parameters. Reduced frequencies between about 0.1 to 1.0 are tested, as well as the limiting case of static thrust that yields a theoretical reduced frequency of infinity (based on free-stream speed). Note, for flapping-wing motions the Strouhal number is generally based on the plunge amplitude, and in that form it is given by $Sr = h_y k$. The Reynolds number is not of great importance to this investigation, but it varied roughly between 18,000 and 80,000, based on chord length.

Numerical Methods

Flow solutions are computed using an unsteady, potential-flow code originally developed by Teng,[27] with a Graphical User Interface (GUI) developed by Jones and Center.[28]

The basic, steady panel code follows the approach of Hess and Smith,[29] where the airfoil is approximated by a finite number of panels, each with a local, uniform, distributed source strength and all with a global, uniform, distributed vorticity strength. For n panels there are n unknown source strengths, q_j, and an unknown vorticity strength, γ. Boundary conditions include flow tangency at the midpoint of the n panels and the Kutta condition which postulates that the pressure on the upper and lower surfaces of the airfoil at the trailing edge must be equal.

The unsteady panel code adopts the procedure of Basu and Hancock,[30] where a wake panel is attached to the trailing edge through which vorticity is shed into the flow. The Helmholtz theorem states that the total vorticity in a flow remains constant, thus a change in circulation about the airfoil must result in the release of vorticity into the wake equal in magnitude and opposite in direction, given numerically by

$$\Delta_k (\gamma_W)_k + \Gamma_k = \Gamma_{k-1} \tag{2}$$

where Δ is the wake panel length, γ_W is the distributed vorticity strength on the wake panel and Γ is the circulation about the airfoil, and where the subscript k indicates the current time step, and $k-1$ indicates the previous time step.

The wake panel introduces two additional unknowns; the wake panel length and its orientation, θ_k, requiring two additional conditions for closure;

1. The wake panel is oriented in the direction of the local resultant velocity at the panel midpoint.
2. The length of the wake panel is proportional to the magnitude of the local resultant velocity at the panel midpoint and the time-step size.

The essential elements of this scheme are summarized in Fig. 9.

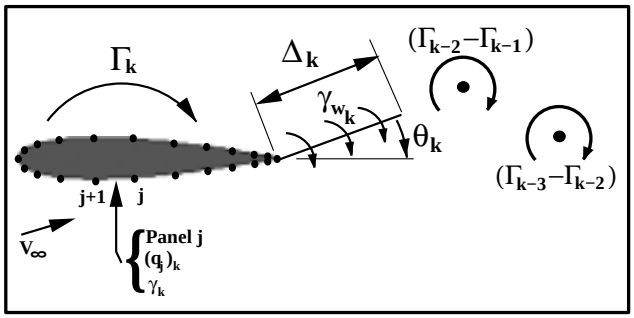

Fig. 9: Schematic of the panel code wake model.

At the end of each time step the vorticity contained in the wake panel is concentrated into a point vortex which is shed into the wake and convected downstream with the flow, influencing and being influenced by the other shed vortices and the airfoil. Note, implementation of this approach requires an iterative scheme, since the velocity direction and magnitude used to define the wake panel are not initially known. Note also that this wake model is nonlinear. The panel method was extended to a two airfoil system by Pang[31], allowing for the computation of wake interference phenomenon. The unsteady panel code has been extensively documented in Refs. 7, 23, 27, 28 and 31-36.

Configurations

Several configurations are used for the experimental and numerical simulations. The equations of motion and parametric nomenclature for the configuration are illustrated in the following figures.

The single airfoil case is shown in Fig. 10. The airfoil shape is arbitrary and has a chord length of 1. The pivot point is located at x_p, measured positive from the leading edge toward the trailing edge.

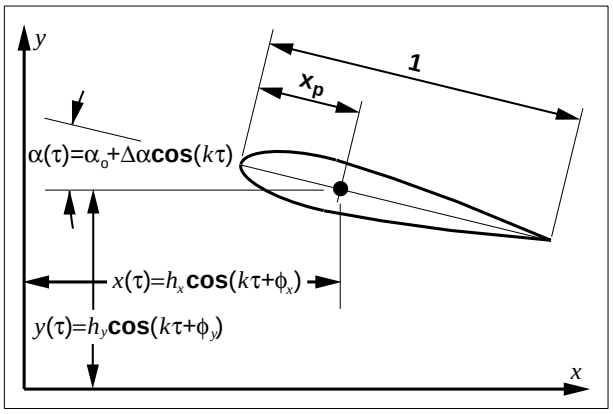

Fig. 10: Single airfoil schematic.

The angle of attack (AOA) and plunge displacements are time-dependent, and are given in the present study as indicated in Fig. 10. While the pitch and plunge amplitudes and the phase angles between the three-degrees-of-freedom may be independently set, the frequency is the same for all three motions (the numerical model can handle different frequencies, but the mechanical flapper cannot).

In Fig. 11 the general two airfoil system is shown. Each airfoil has the same degrees-of-freedom as the single-foil case, but the second foil may have a different chord length, and it is displaced from the first foil by x_0 and y_0.

Using the two-airfoil system, with the airfoils arranged as shown in Fig. 12, and moving the two airfoils anti-symmetrically ($y_2(\tau) = -y_1(\tau)$ and $\alpha_2(\tau) = -\alpha_1(\tau)$), a plane of symmetry is defined between the airfoils, and the system simulates an airfoil in ground effect. The second airfoil becomes an *image-airfoil* within the ground plane. This was studied in some detail in Ref. 23, where it was shown that the propulsive performance of a flapping foil was significantly enhanced near a ground plane. This opposing-plunge or *ground-effect* configuration offers the additional benefits of mechanical and aerodynamic balanced loading in the vertical direction, and is therefore desirable for our wind-tunnel model.

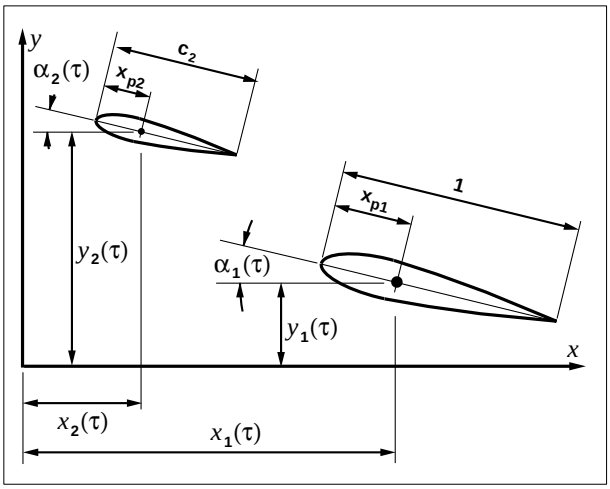

Fig. 11: Two airfoil system.

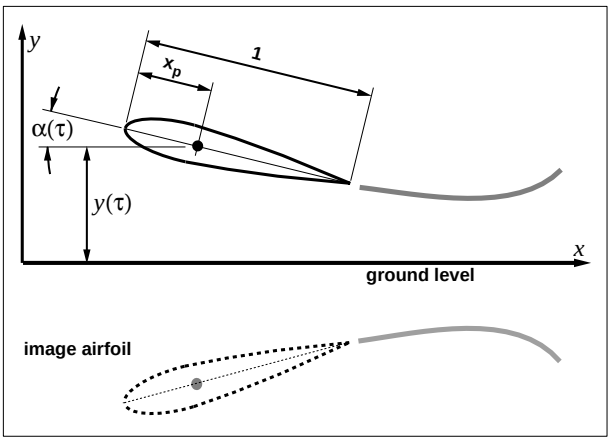

Fig. 12: Airfoil in ground effect.

The numerical and experimental configurations currently tested are illustrated in Fig. 13. The first three (Figs. 13a-c), which require only one or two wing elements, are modeled numerically, and the last three configurations (Figs. 13c-e) are modeled experimentally. With the addition of mechanical counterbalancing to keep the model from shaking itself apart, the first two configurations (Figs. 13a-b) may be experimentally tested in the future.

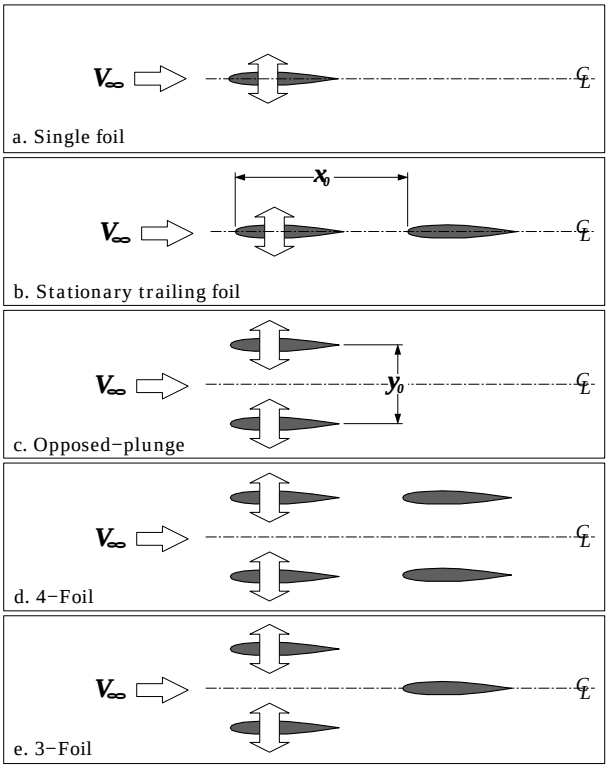

Fig. 13: Numerical and experimental configurations.

As a side note, Schmidt's wave-propeller moved the leading airfoil in a circular path, whereas our mechanical flapper moves the leading airfoil in a linear path, as illustrated in Fig. 13b. However, using the panel code, it was found that virtually identical performance was predicted when the leading airfoil was moved in a circular path or a linear, vertical plunging path.

Results

The panel code has been used in many previous unsteady investigations, and has shown an excellent agreement with linear theory, other numerical methods and experimental results. In Fig. 14, a comparison of the thrust coefficient predicted by linear theory and the panel code for a single flapping airfoil (Fig. 13a), a flapping airfoil with a stationary trailing airfoil (Fig. 13b) and two flapping airfoils in the opposed-plunge formation (Fig. 13c) is shown. In all cases the plunge amplitude was $0.4c$, and the angle of attack was 0 degrees. For the opposed plunge case, the mean distance between airfoils, y_0, was 1.4 chord lengths, and for the stationary trailing airfoil case the trailing distance (LE to LE), x_0, was 1.2 chord lengths (numerical simulations demonstrated minimal dependence on x_0).

The single-airfoil panel code results agree very well with Garrick's linear theory. The thrust coefficient is substantially increased over the full frequency range for the opposed-plunge case; however, the thrust coefficient for the stationary trailing airfoil case (similar to Schmidt's wave propeller) is actually lower than the single-airfoil predictions.

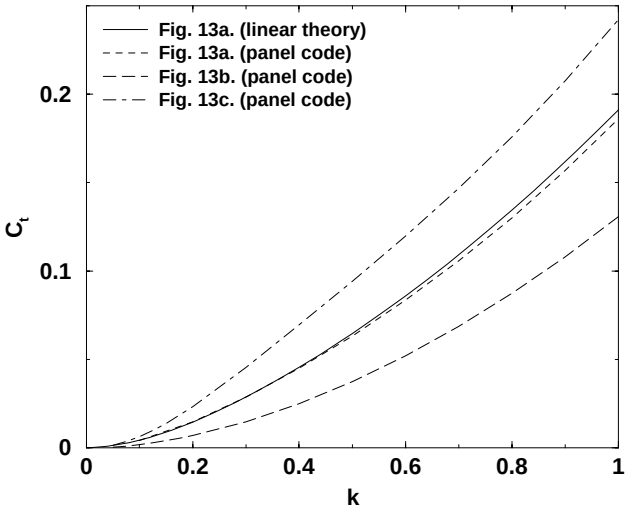

Fig. 14: Thrust coefficient versus reduced frequency.

Note that the thrust coefficient values plotted for the two-airfoil cases are the average of the thrust coefficients for each airfoil. For the opposed-plunge case each foil contributes equally to the thrust, but for the stationary trailing airfoil case, the leading airfoil produces most of the thrust. For the same wetted area, the opposed-plunge case produces roughly twice the thrust as the stationary trailing airfoil configuration.

In Fig. 15 the propulsive efficiency, η_t, is plotted for the cases shown in Fig. 14.

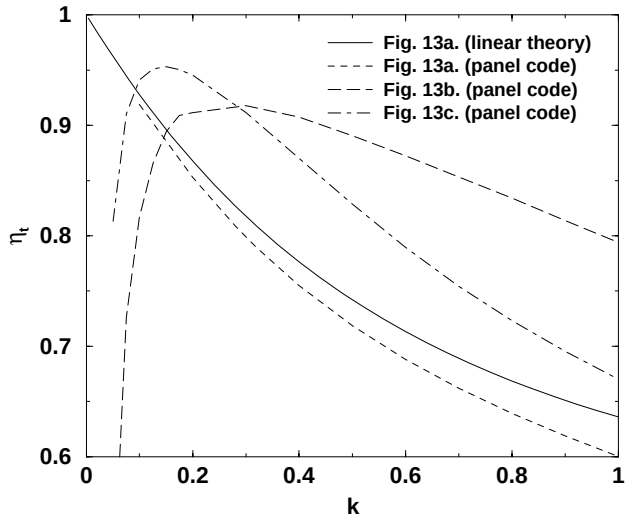

Fig. 15: Propulsive efficiency versus reduced freq.

The stationary trailing airfoil case yields the highest efficiency over most of the frequency range, but

keep in mind that these are inviscid results, and they do not include any viscous drag. Due to the low thrust coefficient of configuration (b), profile drag takes a larger bite out of the propulsive performance, and the stationary trailing airfoil case loses its appeal.

The drop in efficiency at low k, for both of the two-airfoil cases, is probably not real. Both the thrust and power coefficients approach zero at low k, and hence the propulsive efficiency is the ratio of two very small numbers. Any inaccuracy in either C_t or C_p may result in a large error in η_t.

In Fig. 16 the cases shown in Figs. 14 and 15 are presented as real thrust versus flight speed. The geometric parameters are set to match the experimental flapping mechanism, with $c = 64mm$, $b = 1200mm$, $h_y c = 25.4mm$ and $f = 8Hz$. For the two-airfoil cases, this is the thrust per wing, so the total thrust is double the plotted value.

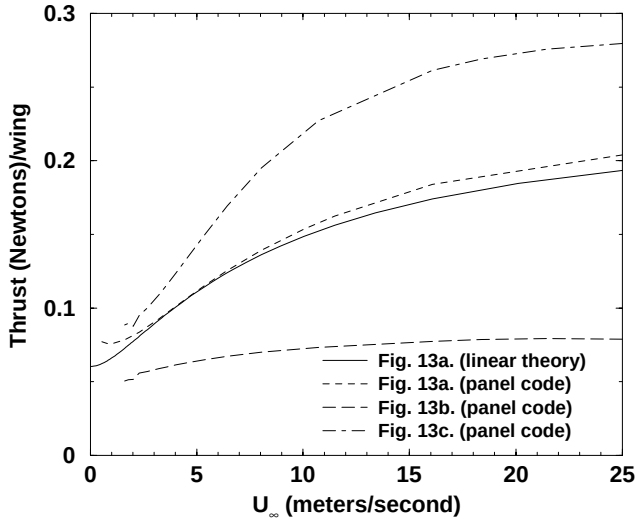

Fig. 16: Thrust versus flight speed.

In Fig. 17 the total thrust predicted by the panel code for the opposing plunge case (Fig. 13c.) and the parameters specified for Fig. 16 is compared to experimentally measured values for several frequencies. As expected, the panel code always predicts thrust values that are greater than the measured values. Note, however, that the steady-state drag has been removed from the plotted experimental thrust values, so the reduction in thrust is primarily due to three-dimensionality effects and flow-separation losses. As expected, the thrust increases rapidly with frequency, roughly as f^2.

In Fig. 18 the effect of mean angle of attack is investigated. The configuration is identical to that used in Figs. 14-17, but the entire mechanism is canted by the indicated angle of attack by adjusting the lengths of the suspension cables.

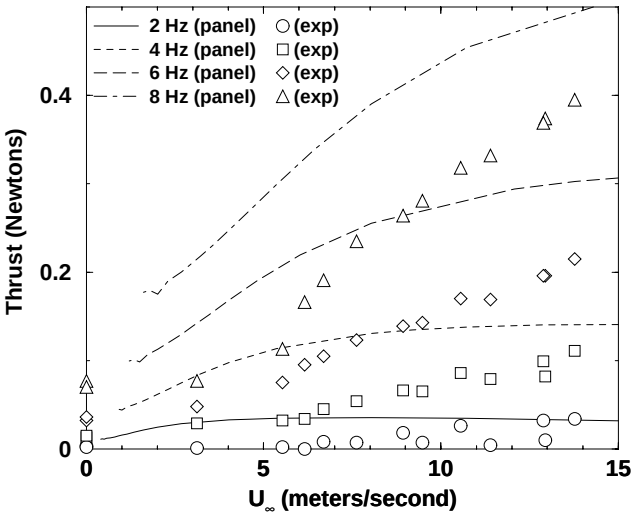

Fig. 17: Thrust versus flight speed for config. c.

Linear theory and the panel code predict very little influence on the thrust due to angle of attack changes, but they do not predict flow separation. As is apparent, with increasing α the thrust remains nearly constant until around $\alpha = 10$ degrees where the thrust rapidly drops off. The plotted results are for $f = 8Hz$. The results at lower frequencies are similar. Note, that at the highest (non-static) reduced frequencies tested, the induced angle of attack due to the plunge motion are on the order of 20 degrees or more, clearly above the steady-state stall angle for the airfoil. The oscillatory dynamics appear to delay massive separation until dynamic angles of attack approaching 30 degrees are reached.

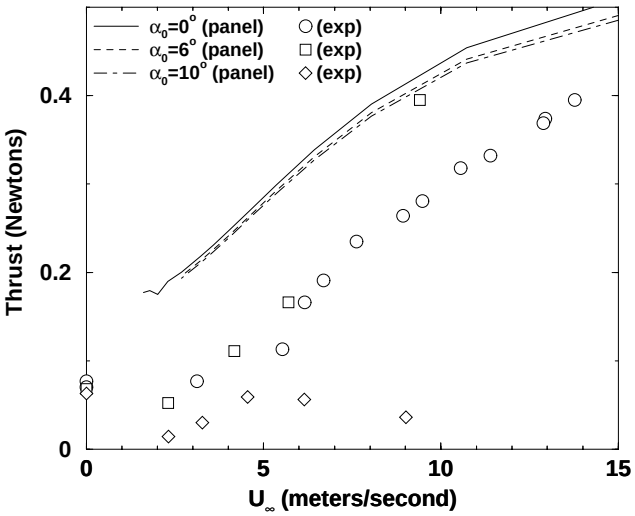

Fig. 18: Thrust versus flight speed and AOA.

In Fig. 19 the measured thrust for several experimental configurations is plotted for $f = 8Hz$. Included are the two-airfoil case (Fig. 13c) and the four-

airfoil case (Fig. 13d) with and without tip-plates. Tip plates were added to the last set to reduce the three-dimensional tip losses, and a marked improvement is seen at lower flight speeds with the tip plates. Note that lower flight speeds correspond to higher reduced frequencies and higher effective angles of attack.

Marginal improvement is predicted for the four airfoil configuration over the full velocity range, but it's important to note that the plotted thrust values have the steady-state drag subtracted, and since the 4-foil cases have a significantly greater wetted area, the increased thrust may be offset by the increased profile drag.

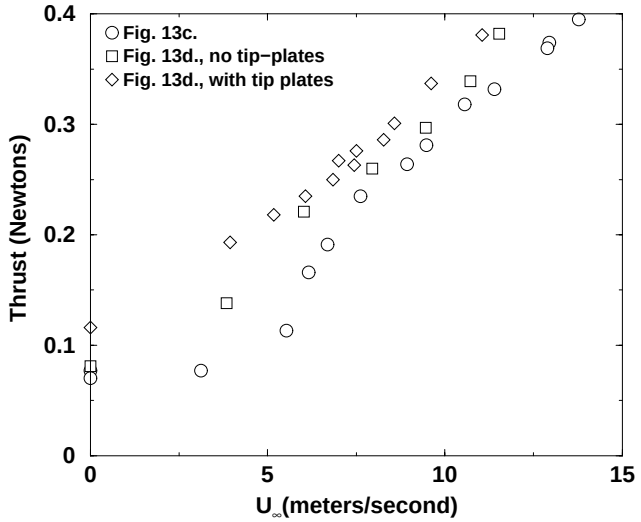

Fig. 19: Thrust versus flight speed for configs. c,d.

The dual-mode (pitch/plunge) parameter space is explored in the next series of plots. In all presented cases, the opposed plunge (Fig. 13c) configuration is used. The mechanics do not provide true sinusoidal pitch/plunge motions, however, for the relatively low pitch amplitudes used here, the deviation is small, and is roughly equivalent to a phase angle, ϕ_y, of -90 degrees and a mid-chord pivot location.

One very notable difference between plunge-only and combined, pitch/plunge flapping is that the thrust for plunge-only flapping asymptotically approaches a positive maximum value as the velocity is increased, whereas the thrust for the dual-mode case becomes negative at a critical velocity. According to linear theory, the thrust changes sign when the induced angle of attack due to the plunge motion equals the geometric pitch angle of attack, resulting in an effective angle of attack of zero. Pitch amplitudes lower than this yield positive thrust, and pitch amplitudes higher than this yield negative thrust or drag. Thus, the dual-mode configuration has a limited velocity range where it is useful for propulsion.

In Fig. 20 the thrust predicted by the panel code is compared to the measured thrust for a configuration with $\Delta\alpha = 3.6$ degrees and $h_y = 0.316$. The agreement at low speeds is remarkably good, but the results at higher speed diverge dramatically with the experimentally measured thrust greatly exceeding the computed thrust. In particular, the zero-thrust velocities found in the experiment are much higher than those predicted by the panel code and linear theory. The obvious explanation is that our experimental conditions did not match our theoretical conditions. Linear theory and the panel code are two-dimensional, but it is highly unlikely that the three-dimensionality of the experiment would lead to an increase in performance.

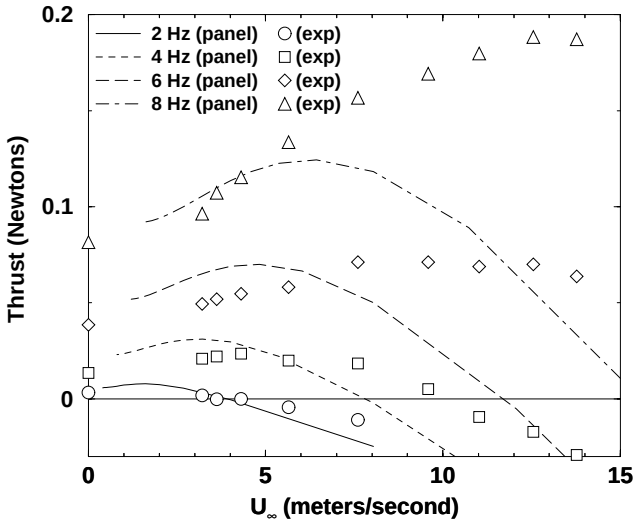

Fig. 20: Dual-mode motion ($\Delta\alpha = 3.6°$, $h_y = 0.316$).

The most likely cause of this error is the flexibility of the wings in the experiment. As previously mentioned, using the strobe light, it was observed that the plunge amplitude at the wing tip greatly exceeded the plunge amplitude at the wing root. At a frequency of 8 Hz, the wing-tips of the upper and lower wings nearly touched, providing a visually estimated tip plunge amplitude of 0.556. The thrust increases roughly as the square of the plunge amplitude, so we would expect nearly 4 times the thrust, plus a greater velocity range where positive thrust is generated. This is shown in Fig. 21 where the root and tip thrust values computed by the panel code are compared to the experimental data for a frequency of 8 Hz.

Clearly, the experimental values fall somewhere between that wide expanse. It's also possible that the wings flex in torsion, but that's much more difficult to measure. The zero-thrust velocity is quite sensitive to the pitch amplitude, so even very small changes in the pitch amplitude will result in very large differences in the measured value.

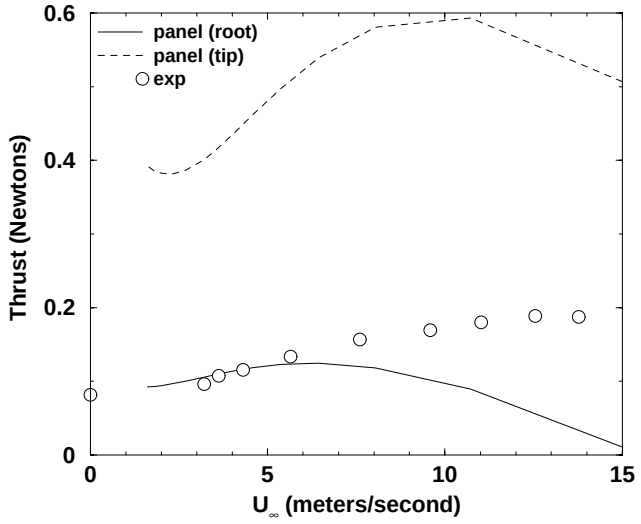

Fig. 21: Thrust based on root and tip motions.

In Fig. 22 the computed and measured thrust values for a case with $\Delta\alpha = 5.0$ degrees and $h_y = 0.335$ are shown for several frequencies. Again, the agreement at low flow velocities is very good, but the flexure of the wings is even more apparent.

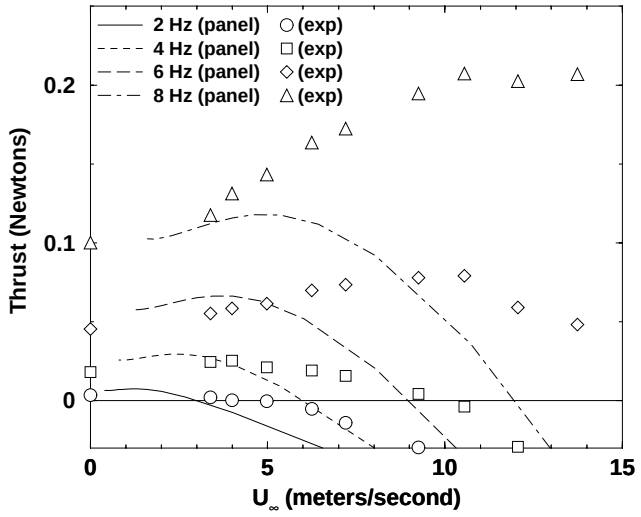

Fig. 22: Dual-mode motion ($\Delta\alpha = 5.0°$, $h_y = 0.335$).

In Fig. 23 the thrust predictions from the panel code for pure plunging and the pitch/plunge motions of Figs. 20 and 22 are compared to the experimental measurements for the 8Hz flapping frequency. Unfortunately, the mechanics of the flapping-wing mechanism make it difficult to keep the plunge amplitude constant while changing the pitch amplitude, but the trends are clear. As the pitch-amplitude is increased the zero-thrust velocity decreases. From the experimental results it can be seen that the static thrust increases with pitch-amplitude. This is expected, since the effective angle of attack is reduced. Actually it's somewhat surprising the the model produces measurable static thrust at all. At zero velocity the effective angle of attack is essentially 90 degrees, and the fact that thrust is produced means that flow separation is favored at the trailing edge, not the leading edge.

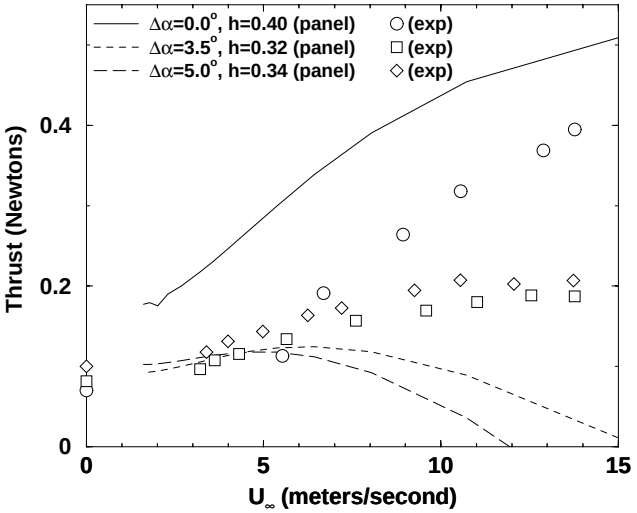

Fig. 23: Thrust versus pitch/plunge-amplitude.

Conclusions

A mechanical flapping-wing device was built, allowing for the systematic evaluation of flapping-wing performance over a broad parameter space. The mechanism flaps two airfoils with variable pitch and plunge amplitude and variable phasing, and allows for the inclusion of additional stationary wings.

Numerical results from a previously developed panel method demonstrate an excellent agreement with linear theory for simple cases, and point out a weakness in Schmidt's wave-propeller concept. While the inviscid propulsive efficiency is high for this configuration, the thrust coefficient is low. The additional, stationary airfoil doubles the wetted area, and therefore the profile drag, and this may offset the slight increase in computed thrust.

Comparisons between the simplified numerical model and the experimental measurements for pure-plunge oscillations demonstrate good qualitative agreement over the full frequency and velocity range. Quantitatively, the panel-code computations over-predict the experimental measurements. This is expected for the opposed-plunge case, considering the three-dimensionality and flow-separation losses that are likely to occur in the wind-tunnel.

Virtually no effect on the thrust was measured for mean angles of attack up to about 6 degrees, but at a mean angle of 10 degrees, the thrust dropped off rapidly, indicating the likely presence of massive flow

separation, a feature that will be investigated in the future with laser-sheet flow visualization.

Experimental measurements of configurations with trailing, stationary wings demonstrate a slight increase in total thrust over the full velocity range, but this benefit was greatly outweighed by the increase in profile drag. The inclusion of tip plates, which reduce the three-dimensional tip-losses, shows an additional increase in total thrust, especially at low frequencies.

For combined pitch/plunge oscillations there are large discrepancies between the panel-code predictions and the measurements which may be due to aeroelastic effects. Further work is required to clarify these aspects.

Acknowledgments

This investigation was supported by the Naval Research Laboratory under project monitor Kevin Ailinger and by the Naval Postgraduate School direct research program. Additional thanks go to John Moulton for his work constructing the model.

References

[1] Knoller, R., "Die Gesetze des Luftwiderstandes," **Flug- und Motortechnik (Wien)**, Vol. 3, No. 21, 1909, pp. 1-7.

[2] Betz, A., "Ein Beitrag zur Erklärung des Segelfluges," **Zeitschrift für Flugtechnik und Motorluftschiffahrt**, Vol. 3, Jan. 1912, pp. 269-272.

[3] Katzmayr, R., "Effect of Periodic Changes of Angle of Attack on Behavior of Airfoils," NACA Report No. 147, Oct., 1922. (translated from **Zeitschrift für Flugtechnik und Motorluftschiffahrt**, March 31, pp. 80-82, and April 13, 1922, pp. 95-101).

[4] Birnbaum, W., "Das ebene Problem des schlagenden Flüels," **Zeitschrift für Angewandte Mathematik und Mechanik**, Vol. 4, No. 4, Aug., 1924, pp. 277-292.

[5] Birnbaum, W., "Der Schlagflügelpropeller und die kleinen Schwingungen elastisch befestigter Tragflügel," **Zeitschrift für Flugtechnik und Motorluftschiffahrt**, Vol. 15, 1924, pp. 128-134.

[6] Von Kármán, T. and Burgers, J. M., "General Aerodynamic Theory - Perfect Fluids," Division E, Vol. II, Aerodynamic Theory, Ed. Durand, W. F., 1943, p. 308.

[7] Jones, K. D., Dohring, C. M. and Platzer, M. P., "Wake Structures Behind Plunging Airfoils: A Comparison of Numerical and Experimental Results," AIAA Paper No. 96-0078, Jan., 1996.

[8] Garrick, I. E., "Propulsion of a Flapping and Oscillating Airfoil," NACA Report 567, 1936.

[9] Theodorsen, T., "General Theory of Aerodynamic Instability and the Mechanism of Flutter," NACA Report No. 496, 1935.

[10] Silverstein, A. and Joyner, U. T., "Experimental Verification of the Theory of Oscillating Airfoils," NACA Report No. 673, 1939.

[11] Bratt, J. B., "Flow Patterns in the Wake of an Oscillating Airfoil," Aeronautical Research Council, R&M 2773, 1953.

[12] Kuchemann, D. and Weber, J., "Aerodynamic Propulsion in Nature," Chapter 11, *Aerodynamics of Propulsion*, McGraw Hill Book Co., New York, 1953, pp. 248-260.

[13] Schmidt, W., "Der Wellpropeller, ein neuer Antrieb fuer Wasser-, Land-, und Luftfahrzeuge," Z. Flugwiss. Vol. 13, 1965, pp. 472-479.

[14] Bosch, H., "Interfering Airfoils in Two-dimensional Unsteady Incompressible Flow," AGARD CP-227, Paper No. 7, Sept. 1977.

[15] DeLaurier, J. D. and Harris, J. M., "Experimental Study of Oscillating-Wing Propulsion," **Journal of Aircraft**, Vol. 19, No. 5, May, 1982, pp. 368-373.

[16] Koochesfahani, M. M., "Vortical Patterns in the Wake of an Oscillating Airfoil," **AIAA Journal**, Vol. 27, No. 9, Sept. 1989.

[17] Liu, P., "Three-Dimensional Oscillating Foil Propulsion," Masters Engineering Thesis, University of Newfoundland, march, 1991.

[18] Liu, P., "A Time-Domain Panel Method for Oscillating Propulsors with Both Chordwise and Spanwise Flexibility," Ph.D. Thesis, University of Newfoundland, 1996.

[19] Send, W., "The Mean Power of Forces and Moments in Unsteady Aerodynamics," **Zeitschrift für Angewandte Mathematik und Mechanik**, Vol. 72, 1992, pp. 113-132.

[20] Send, W., "Otto Lilienthal und der Mechanismus des Schwingenflugs," DGLR-JT96-030, German Aerospace Congress, Dresden, Sept., 1996.

[21] Hall, K. C. and Hall, S. R., "Minimum Induced Power Requirements for Flapping Flight," *Journal of Fluid Mechanics*, Vol. 323, Sept., 1996, pp. 285-315.

[22] Hall, K. C., Pigott, S. A. and Hall, S. R., "Power Requirements for Large-Amplitude Flapping Flight," AIAA Paper No. 97-0827, Jan., 1997.

[23] Jones, K. D. and Platzer, M. F., "Numerical Computation of Flapping-Wing Propulsion and Power Extraction," AIAA Paper No. 97-0826, 1997.

[24] Ringleb, F. O., "The Three-Dimensional Smoke Tunnel of the Naval Air Engineering Laboratory in Philadelphia," Report. NAEL-ENG-6818, Jul. 1961.

[25] Costello, J. P. II, "Smoke and Helium Bubble Visualization Studies of Incompressible Flow Past a Jet-Flap Airfoil," Master's Thesis, Department of Aeronautics and Astronautics, Naval Postgraduate School, Monterey, CA, June 1972.

[26] Pope, A., Wind-Tunnel Testing, Second Edition, John Wiley & Sons, Inc., New York, 1954.

[27] Teng, N. H., "The Development of a Computer Code for the Numerical Solution of Unsteady, Inviscid and Incompressible Flow over an Airfoil," Master's Thesis, Naval Postgraduate School, Monterey, CA, June 1987.

[28] Jones, K. D. and Center, K. B., "Numerical Wake Visualization for Airfoils Undergoing Forced and Aeroelastic Motions," AIAA Paper No. 96-0055, Jan., 1996.

[29] Hess, J. L. and Smith, A. M. O., "Calculation of Potential Flow about Arbitrary Bodies," **Progress in Aeronautical Sciences**, Vol. 8, pp. 1-138, Pergamon Press, Oxford, 1966.

[30] Basu, B. C. and Hancock, G. J., "The Unsteady Motion of a Two-Dimensional Aerofoil in Incompressible Inviscid Flow," **Journal of Fluid Mechanics**, Vol. 87, 1978, pp. 159-168.

[31] Pang, C. K., "A Computer Code for Unsteady Incompressible Flow past Two Airfoils," Aeronautical Engineer's Thesis, Dept. of Aeronautics and Astronautics, Naval Postgraduate School, Monterey, CA, Sept. 1988.

[32] Platzer, M. F., Neace, K. S. and Pang, C. K., "Aerodynamic Analysis of Flapping Wing Propulsion," AIAA Paper No. 93-0484, Jan. 1993.

[33] Neace, K. S., "A Computational and Experimental Investigation of the Propulsive and Lifting Characteristics of Oscillating Airfoils and Airfoil Combinations in Incompressible Flow," Master's Thesis, Dept. of Aeronautics and Astronautics, Naval Postgraduate School, Monterey, CA, Sept. 1992.

[34] Tuncer, I. H., Platzer, M. F. and Ekaterinaris, J. A., "Computational Analysis of Flapping Airfoil Aerodynamics," ASME Fluids Engineering Division, Summer Meeting, June, 1994.

[35] Riester, P. J., "A Computational and Experimental Investigation of Incompressible Oscillatory Airfoil Flow and Flutter Problems," Master's Thesis, Naval Postgraduate School, Monterey, CA, June 1993.

[36] Turner, M., "A Computational Investigation of Wake-Induced Airfoil Flutter in Incompressible Flow and Active Flutter Control," Master's Thesis, Naval Postgraduate School, Monterey, CA, March, 1994.